Nanoparticles of Amorphous Ruthenium Sulfide Easily Obtainable from a TiO_2-Supported Hexanuclear Cluster Complex $[Ru_6C(CO)_{16}]^{2-}$: A Highly Active Catalyst for the Reduction of SO_2 with H_2

Atsushi Ishiguro,[a] Takayuki Nakajima,[a] Tadahisa Iwata,[a] Masahiro Fujita,[a] Taketoshi Minato,[b] Fumitaka Kiyotaki,[b] Yasuo Izumi,*[b] Ken-ichi Aika,[b] Masaya Uchida,[c] Koji Kimoto,[c] Yoshio Matsui,[c] and Yasuo Wakatsuki*[a]

Dedicated to Professor Horst Kisch on the occasion of his 60th birthday

Abstract: TiO_2-supported ruthenium-metal particles were derived from an anionic hexanuclear carbido carbonyl cluster $[Ru_6C(CO)_{16}]^{2-}$ and compared with those prepared conventionally by impregnation of TiO_2 with a solution of $RuCl_3$ followed by reduction with H_2. The average sizes of the metal particles in both systems are similar, that is, 12 Å for molecular cluster-derived particles and 15 Å for those derived from the $RuCl_3$ precursor, although the size distribution is sharper in the former case. These supported particles efficiently promote the reduction of SO_2 with H_2 to give elemental sulfur. Their active form is ruthenium sulfide as confirmed by EXAFS and X-ray diffraction measurements. The nanoscale ruthenium sulfide particles, which originated from the cluster complex, have an amorphous character and show activity even at low temperature (463 K), whereas ruthenium sulfide formed from $RuCl_3$-derived metal dispersion is a pyrite-type RuS_2 crystallite and needs a temperature above 513 K to effect the same catalysis. Amorphous ruthenium sulfide maintains its nano-sized scale ($\approx$14 Å) regardless of the reaction temperature, while RuS_2 crystallite aggregates to form larger nonuniform particles.

Keywords: amorphous materials · cluster compounds · nanostructures · reduction · ruthenium

Introduction

The structures and functions of very small metal particles, which are synthesized with molecular cluster complexes as precursors, have attracted considerable interest.[1] They often show catalytic properties different from conventional supported metals, and this has been attributed to, at least in part, the small size of the catalyst particles. However, most of the reactions examined with such nano-sized fine metal catalysts involve the hydrogenation of olefins, hydroformylations, hydrogenolysis of alkanes, and in some limited cases the reformation of naphtha to produce aromatics. We were originally interested if such a size effect could also be effective in rather drastic reactions, such as SO_2 reduction by H_2, since the catalytic reduction of gaseous SO_2 to elemental sulfur has attracted much attention as a possible strategy to abate SO_2 from combustion processes.[2–5] In our studies along this line, we previously reported that TiO_2-supported ruthenium catalysts, which were prepared from two different precursors, that is, the ruthenium carbido carbonyl cluster complex $[(PPh_3)_2N]_2[Ru_6C(CO)_{16}]$ (**1**) and the metal chloride $RuCl_3$ (**2**), showed the efficient reduction of SO_2 with hydrogen to give elemental sulfur at temperatures higher than 508–513 K.[6] One of the remarkable features of the Ru/TiO_2 catalyst (Ru(**A**)), derived from the cluster complex **1**, was its quite high activity even at a lower temperature of 463–513 K, whereas TiO_2-supported metal particles (Ru(**B**)), made conventionally by the impregnation process from **2**, needed a reaction temperature higher than 513 K (Table 1).

[a] Prof. Dr. Y. Wakatsuki, Dr. A. Ishiguro, Dr. T. Nakajima, Dr. T. Iwata, Dr. M. Fujita
RIKEN (The Institute of Physical and Chemical Research)
Hirosawa 2-1, Wako-shi, Saitama 351-0198 (Japan)
Fax: (+81) 48-462-4665
E-mail: waky@postman.riken.go.jp

[b] Dr. Y. Izumi, T. Minato, F. Kiyotaki, Prof. Dr. K.-i. Aika
Interdisciplinary Graduate School of Science and Engineering
Tokyo Institute of Technology, 4259 Nagatsuta
Midori-ku, Yokohama 226-8502 (Japan)
Fax: (+81) 45-924-5569
E-mail: yizumi@chemenv.titech.ac.jp

[c] Dr. M. Uchida, Dr. K. Kimoto, Dr. Y. Matsui
Advanced Materials Laboratory
National Institute for Materials Science (AML-NIMS)
Tsukuba, Ibaraki, 304-0044 (Japan)
Fax: (+81) 298-51-4976
E-mail: matsui.yoshio@nims.go.jp

  0947-6539/02/0814-3260 $ 20.00+.50/0

Table 1. Reduction of SO_2 with H_2 to elemental sulfur over TiO_2-supported ruthenium catalysts carried out at various temperatures.[a]

Precursor	Conversion [%] T [K]						
	443	463	473	493	503	513	523
1	2.8	81.9	84.3	85.1	86.1	90.1	87.1
2	1.7	1.9	3.2	5.1	9.8	87.6	86.8

[a] See ref. [6] for the reaction conditions.

The metal dispersion on TiO_2 derived from the zero-valent mononuclear complex, that is, [Ru(cyclooctadiene)(cyclooctatriene)], as the precursor exhibited exactly the same temperature dependency as in the case of Ru(**B**), and therefore even if a trace amount of Cl^- ion remains on the metal surface from $RuCl_3$, it should have no effect in the present SO_2 reducing reaction.[6] In this work, the TiO_2-supported particles derived from **1** and **2**, before and after catalysis at various temperatures, were characterized in detail to elucidate the origin of the difference in their activities. Characterization based on transmission electron microscopy (TEM), Ru K-edge X-ray absorption fine structure (EXAFS) spectroscopy, and X-ray diffraction (XRD) measurement indeed showed that Ru(**A**) and Ru(**B**), as well as their sulfide derivative, have significantly different characteristics in the present reaction involving sulfur. However, the main reason for this difference was concluded to be not the size of the catalyst particles, as initially expected, but rather their morphology. The present results suggest the existence of unprecedented amorphous ruthenium sulfide as a nanoparticle dispersion and that it plays a significant role in catalytic activity.

Results

The TiO_2-supported cluster complex was prepared by impregnation of TiO_2 with a solution of **1** in THF and transformed to metal dispersion Ru(**A**) by heating the incipient sample at 573 K for 1.5 h under vacuum and then heating at the same temperature for three hours under a stream of H_2. By using the same procedure, precursor **2** was converted to TiO_2-supported metal dispersion Ru(**B**). The catalytic reduction of SO_2 at T Kelvin was interrupted after two hours, and the gray powders of $[RuS(\mathbf{A})]_T$ and $[RuS(\mathbf{B})]_T$, which were formed from Ru(**A**) and Ru(**B**), respectively, were subjected to EXAFS and XRD spectra measurements, as well as the observation of particle size by TEM.

Transmission electron microscopy: The TEM image of Ru(**A**) (Figure 1a) shows an exceptionally narrow size distribution of metal particles dispersed on TiO_2, with an average size of 12 ± 1.7 Å. The image of Ru(**B**) (Figure 1b) indicates that the average particle size is 15 ± 2.6 Å, and the particles are not as uniform as in the case of Ru(**A**). Energy-dispersive X-ray (EDX) analysis was used to confirm that the dark spots observed were actually images of Ru metal.

When Ru(**A**) was exposed to a gaseous mixture of SO_2/H_2 (1/2 v/v) at 443 K for two hours, only a slight conversion (2.8%) of SO_2 to elemental sulfur was observed (Table 1). However, the particle-size changed during that process: the resulting particles, denoted $[RuS(\mathbf{A})]_{443}$, became smaller (average size 8 ± 2.6 Å), but still maintained a sharp size distribution (Figure 2a). In contrast, upon treating Ru(**B**) under the same conditions, the resulting particle $[RuS(\mathbf{B})]_{443}$ tended to be larger with an even wider distribution compared

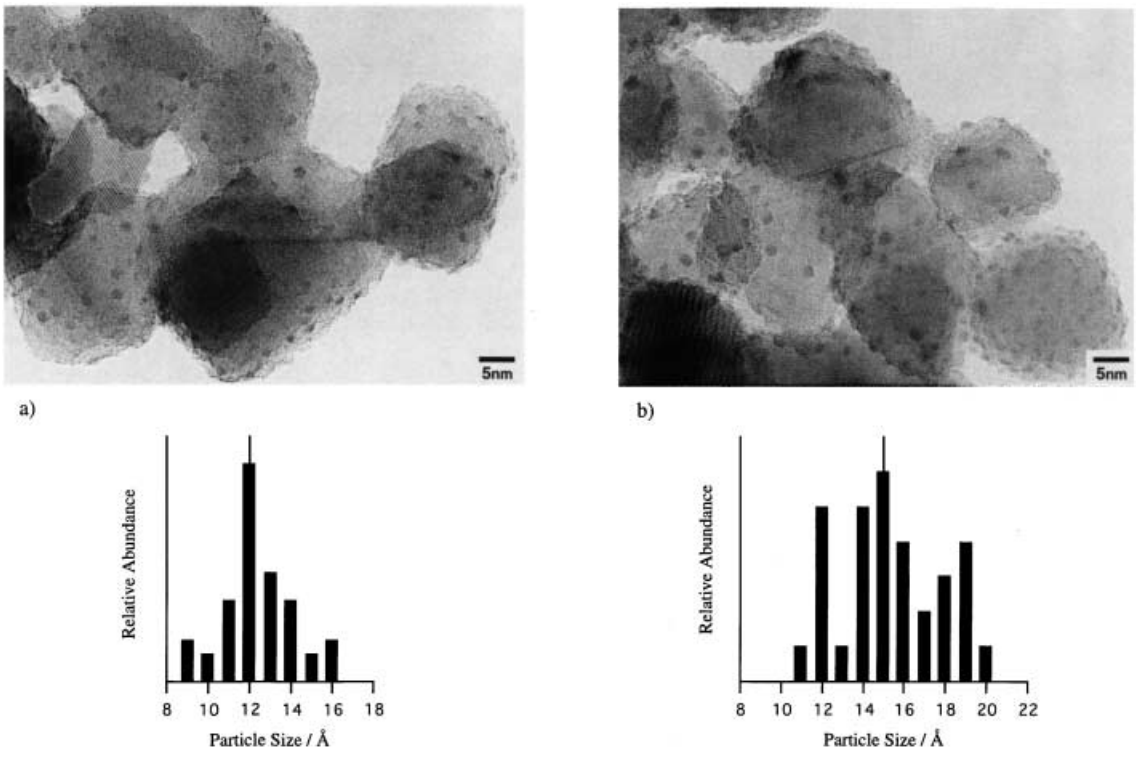

Figure 1. TEM images and histograms of the TiO_2-supported Ru particles. a) Ru(**A**); b) Ru(**B**).

  0947-6539/02/0814-3261 $ 20.00+.50/0

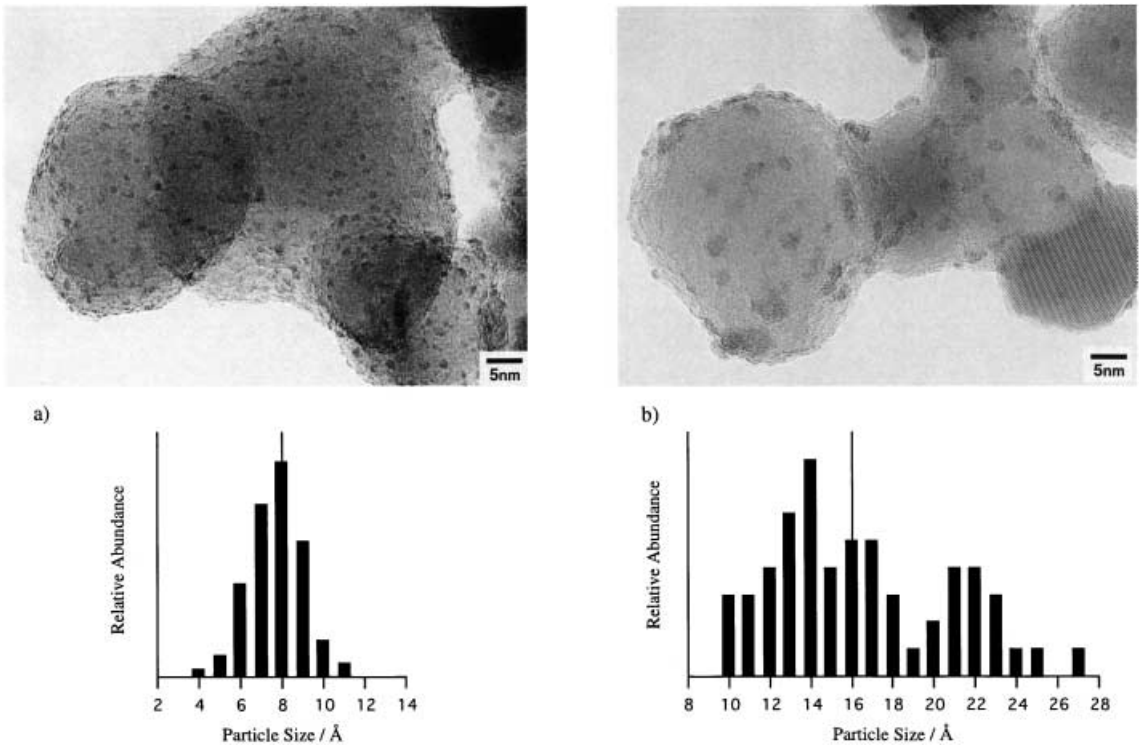

Figure 2. TEM images and histograms of the TiO_2-supported particles obtained from the reaction with SO_2/H_2 at 443 K. a) $[RuS(\mathbf{A})]_{443}$; b) $[RuS(\mathbf{B})]_{443}$.

to that of the parent Ru(**B**) (Figure 2b). This property of [RuS(**B**)] for aggregation is more pronounced at higher temperatures, as shown in Figure 3b: $[RuS(\mathbf{B})]_{473}$ paricles have average sizes of 30 ± 7.8 Å. Likewise, the avarage size for $[RuS(\mathbf{B})]_{523}$ particles was observed to be 30 ± 6.3 Å, which act as a catalyst at 523 K (Table 1). The changes in particle size and distribution with the reaction temperature are much less in the system with Ru(**A**); $[RuS(\mathbf{A})]_{473}$ still has a narrow distribution, with a particle size of 14 ± 1.8 Å (Figure 3a), while $[RuS(\mathbf{A})]_{523}$ has a mean particle size of 14 ± 3.5 Å, as summarized in Table 2.

Ruthenium EXAFS spectra: Figure 4 displays the original raw EXAFS data. Figures 5 and 6 show the normalized

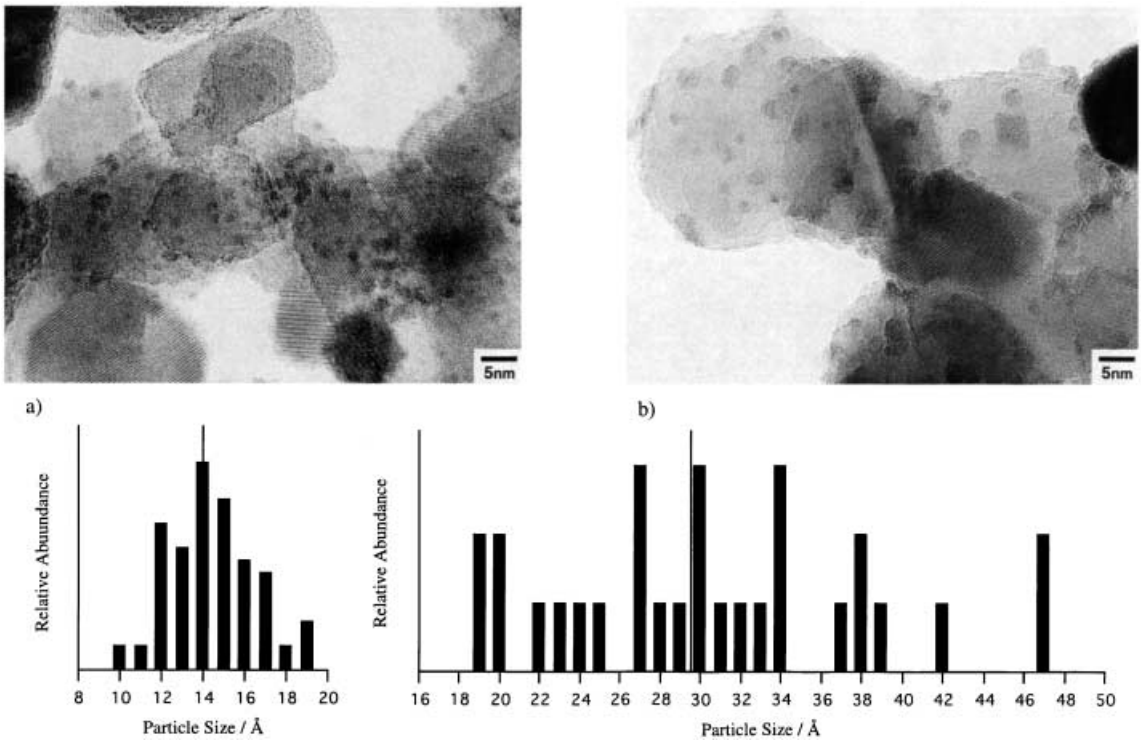

Figure 3. TEM images and histograms of the TiO_2-supported particles obtained from the reaction with SO_2/H_2 at 473 K. a) $[RuS(\mathbf{A})]_{473}$; b) $[RuS(\mathbf{B})]_{473}$.

  0947-6539/02/0814-3262 $ 20.00+.50/0 *Chem. Eur. J.* **2002**, *8*, No. 14

Table 2. Particle size [Å] of Ru-nanoparticles measured from TEM images.

	Before reaction	Reaction temperature [K] 443	473	523
Ru(**A**)	12±1.7			
Ru(**B**)	15±2.6			
$[RuS(\mathbf{A})]_T$		8±2.6	14±1.8	14±2.9
$[RuS(\mathbf{B})]_T$		16±4.6	30±7.8	30±6.5

oscillation $c(k)$ and the associated k^3-weighted Fourier transforms, respectively, for the supported Ru catalysts before (a and e) and after (b–d and f, g) the catalytic run at each reaction temperature. Figure 7 shows the results of respective curve-fitting analysis.

The Fourier transform for the initial metal dispersion of Ru(**A**) exhibits a single strong peak (Figure 6a). By comparison with the EXAFS oscillation and its associated Fourier transform spectra of authentic Ru metal powder, this peak was confirmed to represent the nearest neighboring Ru–Ru bond. TiO_2-supported Ru metal has been reported to lack the Ru–O bond.[7, 8] Furthermore, in the present case, the one-shell Ru–Ru model gave a satisfactory fit, as shown in Figure 7a, while two-shell (Ru–O + Ru–Ru) fitting did not give reasonable parameters. The corresponding Fourier transform for Ru(**B**) (Figure 6e) again has a strong single peak due

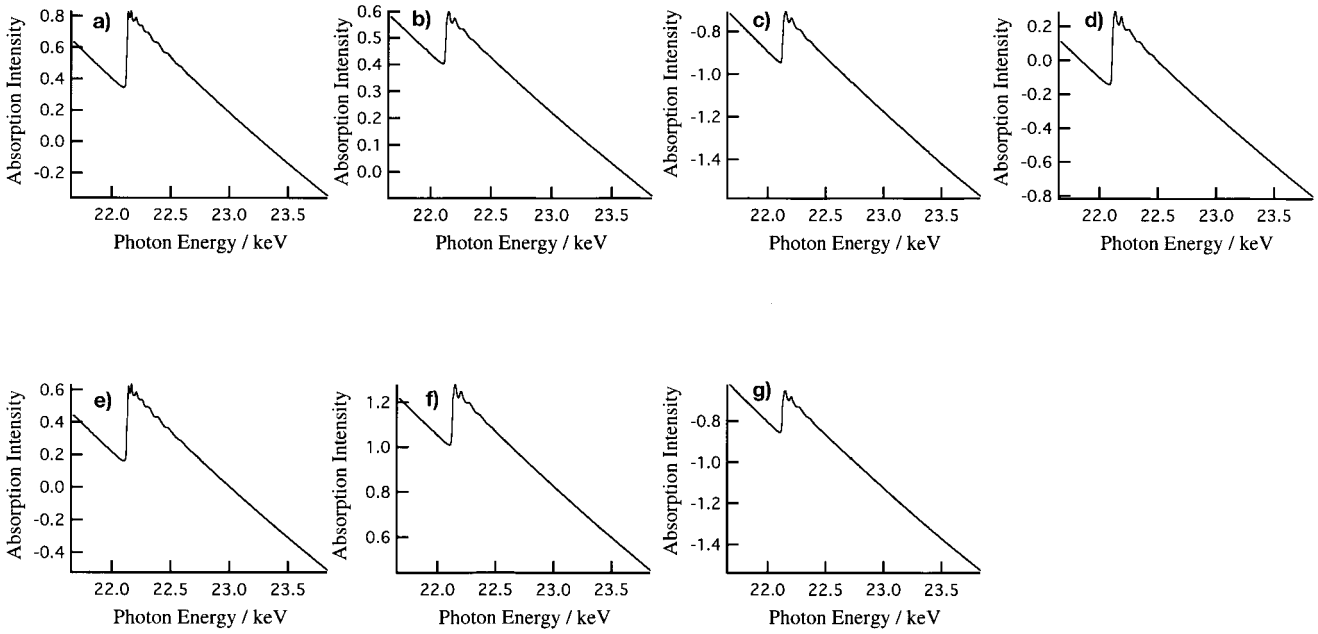

Figure 4. Original Ru K-edge EXAFS data. a) Ru(**A**), b) $[RuS(\mathbf{A})]_{443}$, c) $[RuS(\mathbf{A})]_{473}$, d) $[RuS(\mathbf{A})]_{523}$, e) Ru(**B**), f) $[RuS(\mathbf{B})]_{473}$, and g) $[RuS(\mathbf{B})]_{523}$.

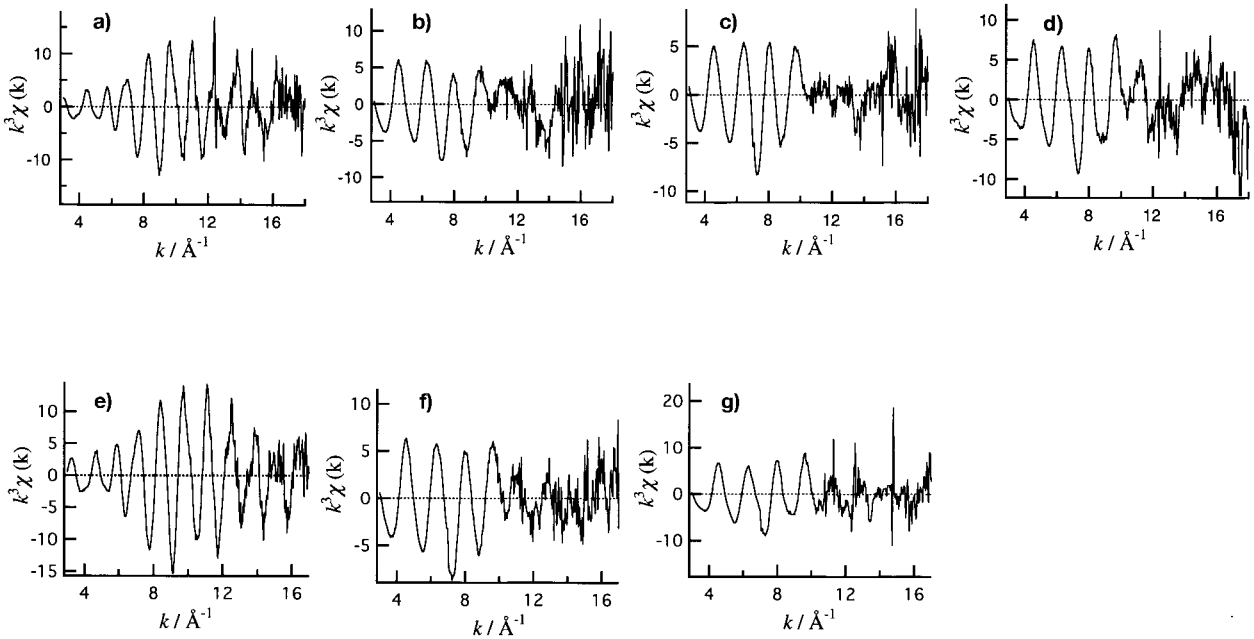

Figure 5. Ru K-edge EXAFS oscillations $\chi(k)$ of a) Ru(**A**), b) $[RuS(\mathbf{A})]_{443}$, c) $[RuS(\mathbf{A})]_{473}$, d) $[RuS(\mathbf{A})]_{523}$, e) Ru(**B**), f) $[RuS(\mathbf{B})]_{473}$, and g) $[RuS(\mathbf{B})]_{523}$.

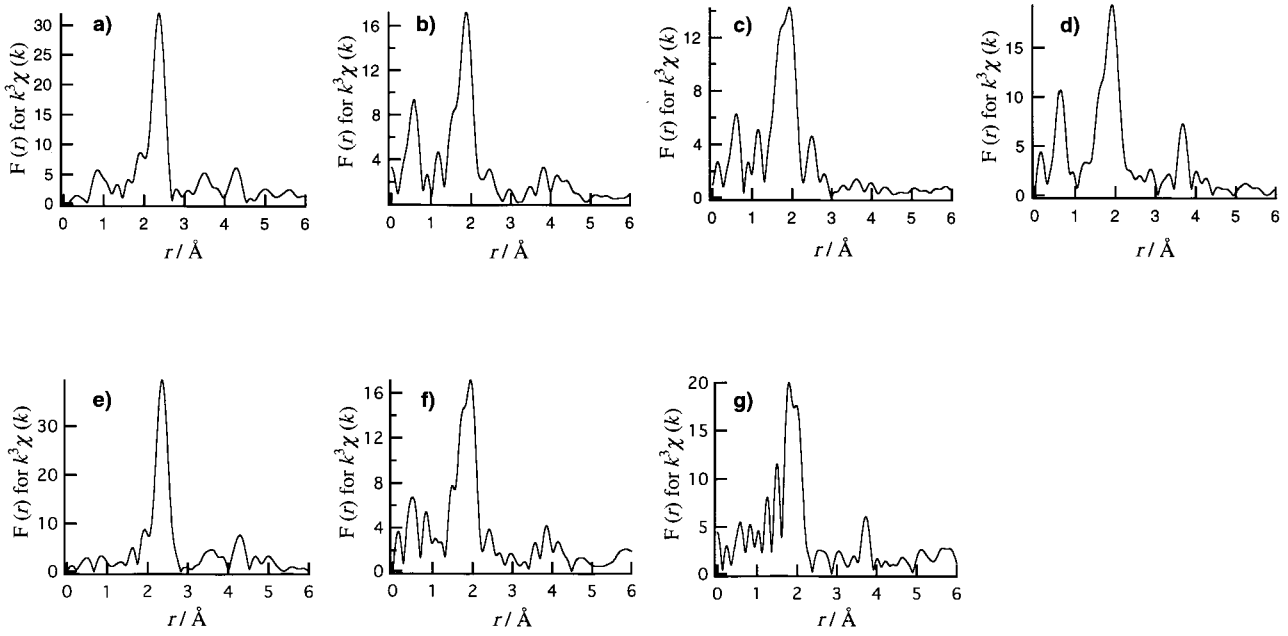

Figure 6. Fourier transforms of k^3-weighted EXAFS data of a) Ru(**A**), b) $[RuS(\mathbf{A})]_{443}$, c) $[RuS(\mathbf{A})]_{473}$, d) $[RuS(\mathbf{A})]_{523}$, e) Ru(**B**), f) $[RuS(\mathbf{B})]_{473}$, and g) $[RuS(\mathbf{B})]_{523}$.

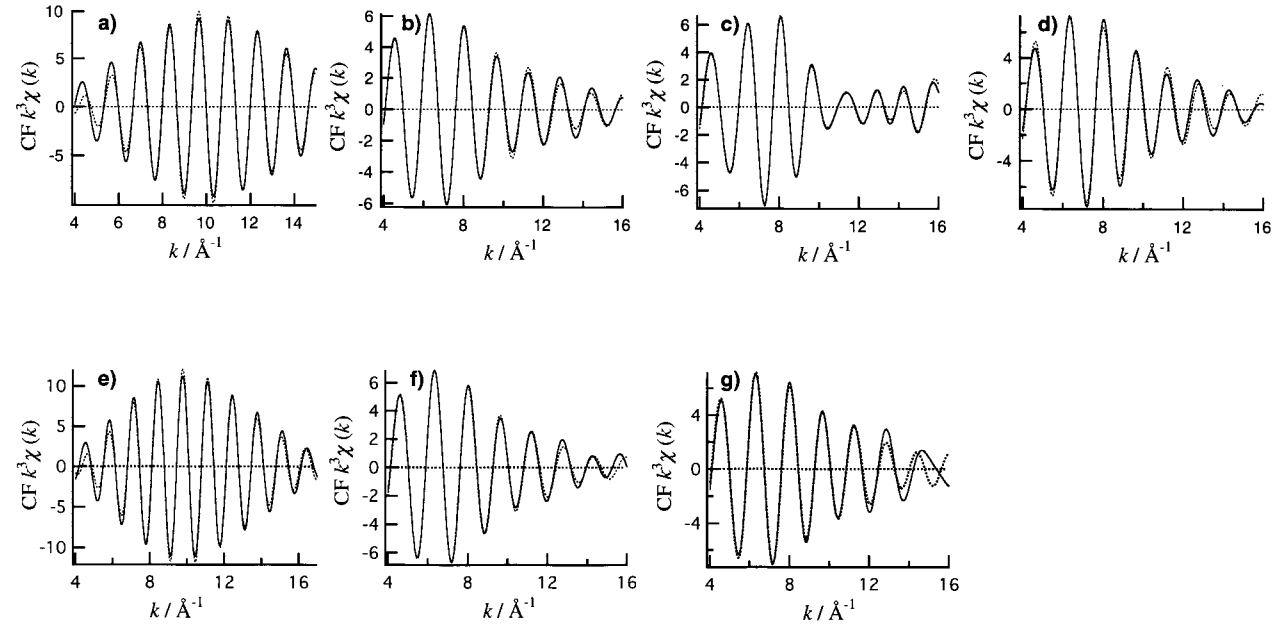

Figure 7. Inverse Fourier transforms (lines) and calculated curve-fitting (dots) of a) Ru(**A**), b) $[RuS(\mathbf{A})]_{443}$, c) $[RuS(\mathbf{A})]_{473}$, d) $[RuS(\mathbf{A})]_{523}$, e) Ru(**B**), f) $[RuS(\mathbf{B})]_{473}$, and g) $[RuS(\mathbf{B})]_{523}$.

to the Ru–Ru bond and agrees well with the EXAFS spectrum reported in the literature for Ru metal supported on TiO_2.[8] Structural parameters are summarized in Table 3.

Table 3. Structural parameters of Ru(**A**) and Ru(**B**) determined from EXAFS data.

	Ru–Ru				R_f [%]
	N	d [Å][a]	ΔE^0 [eV]	$\Delta\sigma$ [Å]	
Ru(**A**)	7.0	2.67	4.9	0.023	1.7
Ru(**B**)	9.2	2.66	9.8	0.037	1.8

[a] The Ru–Ru distance determined by X-ray analysis of the metal is 2.65 Å.

The coordination number of the Ru–Ru bond was 7.0 for Ru(**A**) and 9.2 for Ru(**B**), which is consistent with the smaller size of Ru(**A**) observed by TEM (Table 2).

The Fourier transform of EXAFS data for $[RuS(\mathbf{A})]_{443}$, which is the species formed when Ru(**A**) is treated with a SO_2/H_2 gas mixture at 443 K (Table 1), is shown in Figure 6b. The spectrum is completely different from that of the parent Ru(**A**). The direct Ru–Ru bond is now very weak, while one strong peak is seen for the Ru–S bond, as assigned based on the spectrum of authentic RuS_x ($x \approx 2$). The curve-fitting analysis based on two shells (Ru–S + Ru–Ru) gave the reasonable parameters listed in Table 4, while the fitted curve

  0947-6539/02/0814-3264 $ 20.00+.50/0 *Chem. Eur. J.* **2002**, *8*, No. 14

Table 4. Structural parameters of catalysts [RuS(**A**)] and [RuS(**B**)] determined from EXAFS data.

Catalyst	Ru–S				Ru–Ru				R_f [%]
	N	d [Å][a]	ΔE^0 [eV]	$\Delta\sigma$ [Å]	N	d [Å][a]	ΔE^0 [eV]	$\Delta\sigma$ [Å]	
$[RuS(\mathbf{A})]_{443}$	5.3	2.31	0.1	0.017	0.4	2.72	-6.8	0.020	0.7
$[RuS(\mathbf{A})]_{473}$	3.8	2.33	8.1	0.054	1.6	2.77	6.1	0.199	2.0
$[RuS(\mathbf{A})]_{523}$	6.5	2.33	4.6	0.014	–	–	–	–	1.8
$[RuS(\mathbf{B})]_{473}$	6.0	2.31	1.6	0.020	–	–	–	–	1.3
$[RuS(\mathbf{B})]_{523}$	6.2	2.31	0.3	0.015	–	–	–	–	3.8

[a] The Ru–S distance in pyrite RuS_2 crystals is 2.351 Å.

is shown in Figure 7b. The N_{Ru-Ru} value was only 0.4; the N_{Ru-S} was 5.3. The Ru–S bond length of 2.31 Å is comparable to the corresponding value of 2.351 Å found in the pyrite-type single crystals of RuS_x. At 473 K and 523 K, the cluster-derived particles showed good catalytic activity (Table 1) and the corresponding EXAFS data (Figures 5c, 6c; 5d, 6d) of the supported particles $[RuS(\mathbf{A})]_{473}$ and $[RuS(\mathbf{A})]_{523}$ were essentially the same as those for $[RuS(\mathbf{A})]_{443}$. For the curve-fitting shown in Figure 7d ($[RuS(\mathbf{A})]_{523}$), a one-shell approximation based on Ru–S was good enough (Table 4).

The EXAFS data for $[RuS(\mathbf{B})]_{473}$ and $[RuS(\mathbf{B})]_{523}$, obtained from noncatalytic and catalytic runs, respectively (Table 1), were similar to those of the corresponding [RuS(**A**)] analogues, as shown in Figures 5f–7f and 5g–7g. The Fourier transformed data in the range of 1.5–2.5 Å show a single peak. These were fit (Figure 7f and g) with curves generated using one-shell (Ru–S) parameters (Table 4).

All of these EXAFS data prove that the initially formed TiO_2-supported metal nanoparticles, Ru(**A**) and Ru(**B**), are converted to metal sulfide species upon reacting with a SO_2/H_2 gas mixture above 443 K, regardless of whether the temperature is high enough to achieve active catalysis.

X-ray diffraction (XRD) analysis: Since the metal loading of 1.5 wt % used for TEM and EXAFS studies was too low for XRD measurements, TiO_2 was loaded with the metal in 15 wt %. Figure 8a shows the XRD of blank TiO_2. As expected from the EXAFS data, both $[RuS(\mathbf{B})]_{473}$ and $[RuS(\mathbf{B})]_{523}$ (Figure 8b) show two peaks at $2\theta = 32$ and 46°, which are assignable to the [200] and [220] faces, respectively, of the RuS_2 pyrite phase. The RuS_2 [311] face at $2\theta = 54°$ is overlapped by the strong peaks of TiO_2.

In contrast, both $[RuS(\mathbf{A})]_{503}$ and $[RuS(\mathbf{A})]_{523}$ showed the same XRD pattern (Figure 8e), which had a very broad peak in the range $2\theta = 30–55°$, as is evident by comparison with the XRD pattern of pure TiO_2. Annealing of the $[RuS(\mathbf{A})]_{523}$ sample under Ar at 723 K for two hours (Figure 8d) and further at 773 K for two hours (Figure 8c) yielded a sample with an XRD pattern that was essentially the diffraction of pyrite-type RuS_2 crystallite. To confirm further that the broad XRD peak observed in Figure 8e is due to ruthenium sulfide and not to impurities, a typical sulfidation method with conditions for metals was applied for Ru(**A**), that is, the reaction was performed at 573 K with H_2S/H_2 (1/9 *v*/*v*) in place of SO_2/H_2. The XRD pattern of the resulting ruthenium sulfide had exactly the same broad peak as that in Figure 8e, and annealing of this sample at 773 K gave the expected [200] and [220] peaks of the crystalline RuS_2. Similar sulfidation of

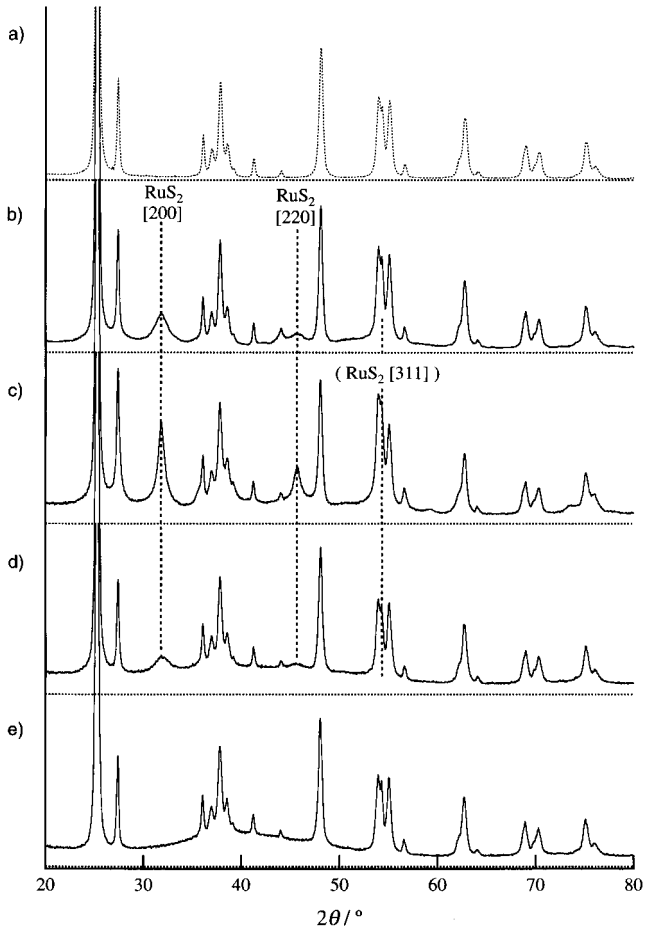

Figure 8. XRD patterns of a) blank TiO_2 sample, b) $[RuS(\mathbf{B})]_{473}$ and $[RuS(\mathbf{B})]_{523}$, c) $[RuS(\mathbf{A})]_{523}$ sample after annealed at 773 K, d) $[RuS(\mathbf{A})]_{523}$ sample after annealed at 723 K, and e) $[RuS(\mathbf{A})]_{503}$ and $[RuS(\mathbf{A})]_{523}$.

Ru(**B**) with H_2S/H_2 proceeded only above 673 K, and its XRD pattern was very close to that shown in Figure 8b. Based on these observations, the broad peak present in Figure 8e is assigned to the amorphous phase of ruthenium sulfide.

XRD peaks of the parent metal dispersions Ru(**A**) and Ru(**B**) could be observed only in low 2θ region due to low intensities of the diffraction. XRD of Ru(**B**) showed, albeit unresolved, overlapped peaks assignable to [002] and [101] faces of the hcp phase of the metal crystallite, whereas the corresponding diffraction for Ru(**A**) is broader and the peak top position is apparently different from those of the authentic Ru metal (Figure 9).

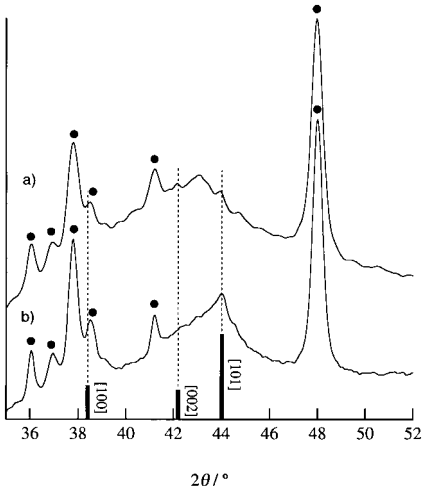

Figure 9. XRD peaks of the TiO_2-supported Ru metal-particles: a) Ru(**A**), b) Ru(**B**). The marked peaks are those due to TiO_2 back-ground.

Discussion

Molecular metal cluster complexes have been used as some of the most effective sources for supported ultimately fine metal particles.[1] With regard to hexaruthenium carbonyl clusters with an interstitial carbide, a methyl derivative $[Ru_6C(CO)_{16}(CH_3)]^-$ has been used as a precursor to bring about strong interaction with the supporting material (MgO, Al_2O_3, TiO_2) and to maintain the $[Ru_6C]$/support structure framework after the organic ligands are removed under vacuum at 523–623 K.[9–11] When the interaction between the metal and the support is not strong enough, aggregation of the initially formed metal cluster particle may take place to some extent. In a series of studies based on the $[PtRu_5C(CO)_{16}]$ complex supported on carbon black, it has been shown that reduction with H_2 at 673 K yields bimetallic nanoparticles (average diameter of 16 Å) with a narrow size distribution packed in an fcc structure rather than a conventional hcp structure.[12–14] In the case of the present dispersed metal Ru(**A**) derived from impregnated **1** in 1.5 wt%, it is evident that some aggregation also occurred during treatment for decarbonylation at 573 K. The TEM study indicates that the average size of Ru(**A**) is 12 Å with a significantly narrow size distribution, which roughly corresponds to the condensation of five $[Ru_6]$ metal units. By similar treatment of the metal chloride precursor **2**, dispersed metal Ru(**B**), with an average diameter of 15 Å, is obtained (Figure 1). Although the size distribution of Ru(**A**) is markedly sharper than that of Ru(**B**), it is difficult to explain the difference in the catalytic reactivity for SO_2 reduction (Table 1) by this difference in the size of these metal particles.

The Ru K-edge EXAFS spectra suggest that when a gas mixture of SO_2/H_2 (1/2 v/v) is passed over these supported ruthenium-metal particles at temperatures higher than 443 K, the Ru–Ru bond is almost completely lost, while ruthenium sulfide becomes the predominant chemical component. Thus, the active catalyst species in the reduction of SO_2 with H_2 is confirmed to be ruthenium sulfide. Therefore, the ruthenium sulfide [RuS(**A**)], which originates from cluster complex **1** and is formed in the SO_2 reducing reaction of metal Ru(**A**), is highly active as a catalyst at a low temperature of 463–503 K. In contrast, the other ruthenium sulfide [RuS(**B**)], formed from Ru(**B**), is inactive in the same temperature range (Table 1) and works only at higher temperatures.

XRD can provide information on structural differences between the two ruthenium sulfides. Sulfide [RuS(**B**)] is evidently an ubiquitous pyrite-type crystallite of RuS_2 supported on TiO_2, while [RuS(**A**)] is amorphous (Figure 8). Successful curve-fitting analysis of the EXAFS data for [RuS(**A**)], with calculations based on crystalline RuS_2 (Figure 7), suggests that the relative orientation of the Ru and nearest S atoms in the amorphous phase is similar to that in the more common pyrite-type form (Table 4). Although there have been a number of reports concerning Ru sulfide, only two have reported the preparation of an amorphous form.[15, 16] The reported XRD of amorphous Ru sulfide consists of two broad overlapping humps with 2θ ranging from approximately 20–55°, although the peak-head positions are evidently different in the two reports. To the best of our knowledge, [RuS(**A**)] obtained in the present study is the first example of a supported amorphous species of a ruthenium sulfide dispersion and also the first case in which reactivity of amorphous ruthenium sulfide was examined.

Comparison of the ruthenium sulfides prepared here by TEM indicates that the sulfidation of Ru(**A**) during the reaction with SO_2/H_2 causes partial fragmentation of the metal particles into smaller metal sulfide particles at low temperature, that is, $[RuS(\mathbf{A})]_{443}$ has an average size of 8 Å (Figure 2a). Although some re-aggregation takes place at higher temperatures, the particle size remains rather small, for example, $[RuS(\mathbf{A})]_{473}$ and $[RuS(\mathbf{A})]_{523}$ each measured $\approx$14 Å (Table 2). Thus, it is very likely that amorphous ruthenium sulfide [RuS(**A**)] has weak interaction between the RuS_2 units, which does not allow greater aggregation. In the case of Ru(**B**), the behavior toward sulfidation through the reaction with SO_2/H_2 is very different from that with Ru(**A**); at 443 K, the reaction induced partial aggregation rather than fragmentation and resulted in a broad distribution of the particle size of 20–25 Å (Figure 2b). The tendency of crystalline RuS_2 for rather random aggregation is even more pronounced at higher temperature, at which it gives ruthenium sulfide [RuS(**B**)] with the particle size scattered over a wide range of 18–47 Å (473 K) and 17–33 Å (523 K), as shown in Figure 3b.

The striking difference between the two ruthenium sulfide catalysts, one originating from the $[Ru_6]$ cluster complex **1** and the other from ruthenium salt **2**, may be traced back to the different morphologies of the initially formed metal particles Ru(**A**) and Ru(**B**), which are intermediate precursors for the sulfide species. Aside from sulfidation by a gas mixture of SO_2/H_2 (1/2 v/v) as discussed above, the more common sulfidation process with a gas mixture of H_2S/H_2 (1/9 v/v) also gave amorphous ruthenium sulfide from Ru(**A**) and pyrite-type crystallite from Ru(**B**), as observed by XRD analysis (Figure 8). Furthermore, the fact that a higher temperature is needed for the sulfidation of Ru(**B**) (673 K) by H_2S/H_2 relative to the reaction with Ru(**A**) (573 K) is another indication of the higher reactivity of Ru(**A**). The

  0947-6539/02/0814-3266 $ 20.00+.50/0 *Chem. Eur. J.* **2002**, *8*, No. 14

XRD observations displayed in Figure 9 suggest that TiO_2-supported Ru(**A**) and Ru(**B**) vary with regard to structure: Ru(**A**) is much more reactive probably because it has significant structural defects or more amorphous-like, compared to crystalline metal Ru(**B**), and furnishes nanoparticles of amorphous metal sulfide on sulfidation.

Conclusion

By comparing the TiO_2-supported metal particles Ru(**A**) and Ru(**B**) and their sulfide derivatives [RuS(**A**)] and [RuS(**B**)], several features became clear.

1) Though the size distribution is sharper in Ru(**A**), the average particle size of the two forms is rather similar (Ru(**A**) 12 Å, Ru(**B**) 15 Å). However, they differ in structures; Ru(**A**) probably has significant structural defects, while Ru(**B**) is a conventional hcp crystallite.
2) Ru(**A**) readily undergoes sulfidation with a H_2S/H_2 gas mixture at 573 K to give amorphous ruthenium sulfide, while Ru(**B**) requires a temperature of 673 K and gives ruthenium sulfide in the form of pyrite-phase crystallite.
3) Upon reaction with a gas mixture of SO_2/H_2, both metal species are converted to Ru sulfide. Ru sulfide derived from Ru(**A**) consists of amorphous RuS_2, while Ru(**B**) gives the conventional RuS_2 pyrate phase. The amorphous ruthenium sulfide formed in situ from Ru(**A**) catalyzes the reduction of SO_2 to elemental sulfur by H_2 at a much lower temperature (463 K) than does the crystalline ruthenium sulfide derived from Ru(**B**) (513 K).
4) Ruthenium sulfide crystallite [RuS(**B**)] aggregates to a larger and nonuniform dispersion at higher temperature. In contrast, amorphous ruthenium sulfide [RuS(**A**)] maintains a small particle size under various temperatures for the catalytic reaction. This probably is due to the much weaker interunit interaction among RuS_2 units in the amorphous phase.
5) Ru EXAFS analysis suggests that the relative orientation of Ru and S atoms in the RuS_2 species of the amorphous phase is similar in average to that in the crystalline pyrite phase.

Ruthenium cluster complexes are thus good precursors for amorphous metal sulfide supported on TiO_2, which is expected to have high activity under rather mild conditions. Further studies on its reactivity in other catalytic reactions are now in progress.

Experimental Section

Sample Preparation: The anionic carbido carbonyl cluster complex, $[(PPh_3)_2N]_2[Ru_6C(CO)_{16}]$ (**1**), was prepared by the method described in the literature.[17] Cluster **1** was supported on TiO_2 (Japan Aerosil P25, mean particle size 21 nm) by impregnation at 298 K for 1 h with dry THF solution under an Ar atmosphere, and subsequent removal of THF in vacuo. The amount of Ru metal loaded was fixed at 1.5 wt% unless stated otherwise. Dried incipient catalysts were heated in vacuum for 1.5 h at 573 K and then reduced for 3 h under a stream of hydrogen at 573 K to give Ru(**A**). In the same manner, $RuCl_3 \cdot 3H_2O$ (**2**) on TiO_2 was reduced to give Ru(**B**). The catalytic reduction of SO_2 was carried out in a gas flow system (flow rate 60 $cm^3 min^{-1}$) as described in a previous report.[6] After the catalytic reaction, elemental sulfur remaining on the catalyst surface was flushed with argon for 2 h at the reaction temperature. The supported catalyst sample was then transferred under Ar to a glass cell with Kapton films on both sides and subjected to EXAFS measurements. Sulfidation of the supported metals Ru(**A**) and Ru(**B**) by H_2S was carried out under a mixture of H_2S/H_2 (1/9 v/v), with a flow rate of 44 $cm^3 min^{-1}$ at atmospheric pressure. In this manner, Ru(**A**) and Ru(**B**) underwent sulfidation at 573 K and 673 K, respectively. After 3 h, the sample was cooled to room temperature and flushed with nitrogen for 1 h.

EXAFS measurements and analysis: Ru K-edge EXAFS measurements were performed at room temperature at beamline 10B of the Photon Factory at the High Energy Accelerator Research Organization (KEK-PF) in Tsukuba. The accumulation ring energy was 2.5 GeV and the ring current was 450–300 mA. The beamline 10B makes use of the channel-cut double crystal monochrometer of Si(311). The incident and transmitted X-rays were monitored by ion chambers filled with Ar for I_0 and Kr for I. The photon energy was calibrated by equalizing the derivative maximum of the absorption edge of Ru powder at 22119.3 eV. The background was subtracted by fitting the polynomial to the pre-edge region and extrapolating it to the postedge region. The edge jump of the subtracted spectrum was normalized at 22131.8 eV.

The EXAFS data were analyzed by the EXAFSH program.[18] Background subtraction was performed by calculating the three-block cubic spline, followed by normalization using the Victoreen parameter. Fourier transformation of the k^3-weighted c function was carried out over the range $k_{min} = 3$ and $k_{max} = 17.0 - 19.0$ $Å^{-1}$ according to the signal/noise (S/N) of each spectrum. The window function (Hanning function) was multiplied by the k width of $(k_{max} - k_{min})/20$ on both ends of the FT k range. Inverse FT was performed in the r range of $r_{min} = 1.3 - 1.4$ and $r_{max} = 3.9 - 4.1$ Å multiplied by the window Hanning function with width 0.1 Å on both ends. Curve-fitting analysis was performed by using a method based on the formula of the plane wave single-scattering theory, with empirical phase shift and amplitude functions extracted from ruthenium metal powder for the Ru–Ru bond (metallic), from RuO_2 for the Ru–O bond, and from RuS_x ($x \approx 2$) for the Ru–S bond. The coordination number (N), bond length (d) and Debye–Waller factor (σ) were determined in the fitting procedure. In Tables 3 and 4, Debye-Waller factors thus obtained are listed in the form of $\Delta\sigma$ in Å, that is, with reference to the corresponding values for the standard compounds (Ru metal, RuO_2, and RuS_2).

Transmission electron microscopy: Microscopy studies were performed by using a field emission Vacuum Generator JEM-2000EXII operated at 200 kV. The spatial resolution of the microscope was estimated to be ~3 Å. Specimens were prepared by dipping a copper-mesh-supported holey carbon grid into an ethanol suspension of the sample.

X-ray diffraction measurement: The amount of Ru metal loaded on TiO_2 was 15 wt% in XRD studies. XRD analysis of the catalyst samples ([RuS(**A**)] and [RuS(**B**)]) was performed on a MAC Science M18XHF X-ray diffractometer with rotating anode generators and a monochromatic detector. $Cu_{K\alpha}$ radiation ($\lambda = 1.542$ Å) was used at 45 kV and 400 mA. For crystal phase identification, the typical operation parameters were divergence slit of 1°, scattering slit 1°, receiving slit 0.3 mm, and a scanning rate of 2° min^{-1} with a 0.02° data interval. XRD patterns were collected in the 2θ domain ranging from 10 to 100°. XRD measurement of intermediate metal particles (Ru(**A**) and Ru(**B**)) was carried out on a Rigaku RINT/RAPID diffractometer with $Cu_{K\alpha}$ ($\lambda = 1.542$ Å) radiation at 40 kV/36 mA with radiation time of 15 min.

Acknowledgement

Finantial support of this work by Eco-molecular Science Program at RIKEN is gartefully acknowledged. The authors appreciate the help of Dr. M. Saigo for the XRD analysis on the dispersed metal particles.

[1] B. C. Gates, *Chem. Rev.*, **1995**, *95*, 511.
[2] S. C. Paik, J. S. Chung, *Appl. Catal. B* **1995**, *5*, 233.
[3] J. Ma, M. Fang, N. T. Lau, *J. Catal.* **1996**, *158*, 251.
[4] T. Zhu, L. Kundakovic, A. Dreher, M. Flytnani-stephanopoulos, *Catal. Today* **1999**, *50*, 381.

[5] S. C. Paik, J. S. Chung, *Appl. Catal. B* **1996**, *8*, 267.
[6] A. Ishiguro, Y. Liu, T. Nakajima, Y. Wakatsuki, *J. Catal.* **2002**, *647*, 61.
[7] Y. Izumi, T. Chihara, H. Yamazaki, Y. Iwasawa, *J. Phys. Chem.* **1994**, *98*, 594.
[8] T. Mizushima, K.Tohji, Y. Udagawa, A. Ueno, *J. Am. Chem. Soc.* **1990**, *112*, 7887.
[9] Y. Izumi, T. Liu, K. Asakura, T. Chihara, H. Yamazaki, Y. Iwasawa, *J. Chem. Soc. Dalton Trans.* **1992**, 2287.
[10] Y. Izumi, T. Chihara, H. Yamazaki, Y. Iwasawa, *J. Am. Chem. Soc.* **1993**, *115*, 6462.
[11] Y. Izumi, T. Chihara, H. Yamazaki, Y. Iwasawa, *J. Phys. Chem.* **1994**, *98*, 594.
[12] M. S. Nahner, A. I. Frenkel, D. L. Adler, J. R. Shapley, R. G. Nuzzo, *J. Am. Chem. Soc.* **1997**, *119*, 7760.
[13] M. S. Nahner, A. I. Frenkel, D. Somerville, C. W. Hills, J. R. Shapley, R. G. Nuzzo, *J. Am. Chem. Soc.* **1998**, *120*, 8093.
[14] C. W. Hills, M. S. Nashner, A. I. Frenkel, J. R. Shapley, R. G. Nuzzo, *Langmuir* **1999**, *15*, 690.
[15] J. D. Passaretti, R. C. Collins, A. Wold, R. R. Chianelli, T. A. Pecorara, *Mater. Res. Bull.* **1979**, *14*, 1167.
[16] P. Jeevanandam, Yu. Koltypin, Y. Gofer, Y. Diamant, A. Gedanken, *J. Mater. Chem.* **2000**, *10*, 2769.
[17] C. T. Hayward, J. R. Shapley, *Inorg. Chem.* **1982**, *21*, 3816.
[18] T. Yokoyama, H. Hamamatsu, T. Ohta, University of Tokyo (Japan), **1994**.

Received: December 27, 2001 [F3764]

  0947-6539/02/0814-3268 $ 20.00+.50/0